

Vector Exceptional Points with Strong Superchiral Fields

Tong Wu,^{1,*} Weixuan Zhang,^{1,*} Huizhen Zhang,^{1,*} Saisai Hou,¹ Guangyuan Chen¹,¹ Ruibin Liu,¹
 Cuicui Lu,¹ Jiafang Li,¹ Rongyao Wang,¹ Pengfei Duan,² Junjie Li,³ Bo Wang,⁴ Lei Shi,⁴
 Jian Zi,⁴ and Xiangdong Zhang^{1,†}

¹Key Laboratory of Advanced Optoelectronic Quantum Architecture
 and Measurements of Ministry of Education, Beijing Key Laboratory of Nanophotonics and
 Ultrafine Optoelectronic Systems, School of Physics, Beijing Institute of Technology, Beijing 100081, China

²CAS Center for Excellence in Nanoscience, CAS Key Laboratory of Nanosystem and
 Hierarchical Fabrication, National Center for Nanoscience and Technology (NCNST), Beijing 100190, China

³Beijing National Laboratory for Condensed Matter Physics, Institute of Physics,
 Chinese Academy of Sciences, Beijing 100190, China

⁴State Key Laboratory of Surface Physics, Key Laboratory of Micro- and
 Nano-Photonic Structures (Ministry of Education) and
 Department of Physics, Fudan University, Shanghai 200433, China



(Received 14 November 2019; accepted 6 February 2020; published 26 February 2020)

Exceptional points (EPs), branch points of complex energy surfaces at which eigenvalues and eigenvectors coalesce, are ubiquitous in non-Hermitian systems. Many novel properties and applications have been proposed around the EPs. One of the important applications is to enhance the detection sensitivity. However, due to the lack of single-handed superchiral fields, all of the proposed EP-based sensing mechanisms are only useful for the nonchiral discrimination. Here, we propose theoretically and demonstrate experimentally a new type of EP, which is called a radiation vector EP, to fulfill the homogeneous superchiral fields for chiral sensing. This type of EP is realized by suitably tuning the coupling strength and radiation losses for a pair of orthogonal polarization modes in the photonic crystal slab. Based on the unique modal-coupling property at the vector EP, we demonstrate that the uniform superchiral fields can be generated with two beams of lights illuminating the photonic crystal slab from opposite directions. Thus, the designed photonic crystal slab, which supports the vector EP, can be used to perform surface-enhanced chiral detection. Our findings provide a new strategy for ultrasensitive characterization and quantification of molecular chirality, a key aspect for various bioscience and biomedicine applications.

DOI: 10.1103/PhysRevLett.124.083901

Chirality plays a crucial role in modern biochemistry and the evolution of life [1,2]. Many biologically active molecules are chiral, and detecting and characterizing chiral enantiomers of these biomolecules are of considerable importance for biomedical diagnostics and pathogen analyses [3–5]. The molecular chirality discrimination can be realized with circular dichroism (CD) spectroscopy describing the difference in molecular absorption of left- and right-handed circularly polarized lights (CPLs) [6,7]. In general, the molecular CD signal is typically weak; thus, chiral analyses by such a spectroscopic technique have usually been restricted to analysis at a relatively high concentration [8–11]. Early works proposed by Tang and Cohen [12,13] have shown that the enantioselectivity of optical excitation of a molecule is highly dependent on the chirality of the optical field, and so it stands that the superchiral field, which possesses larger optical chirality than CPLs, can lead to significant enhancement of enantioselective excitation of chiral molecules, allowing for

ultrasensitive detection and characterization of chiral molecules. Remarkably, the potential of superchiral fields is far more beyond enhancing the difference of absorption between enantiomers, it triggers the development of almost all the spectroscopy technologies related to the optical activity phenomenon, from Raman optical activity and fluorescence CD to optical rotation. The superchiral field can also enhance the difference between total optical forces on enantiomers, which promises the development of application for chiral molecule sorting. Recent investigation has shown that the superchiral field has a potential application in the enantioselective conversion in reactions [14], extending its use from the all-optical areas to photochemistry fields. Because of its high importance in all these applications, the superchiral field has bloomed in the last ten years, and intense theoretical and experimental studies have been devoted to the generalization of strong superchiral near fields with the help of artificial nanostructures [15–25]. Despite this progress, many schemes suffer from

high optical losses [15–25], extrinsic CD caused by the nanostructure itself [24], and different handedness of chiral near fields [15–25]. Thus, how to engineer the achiral nanostructure to produce strong single-handed superchiral fields remains challenging.

On the other hand, in contrast to Hermitian systems, special degeneracies called exceptional points (EPs) widely exist in the non-Hermitian systems [26–28]. Both the real and imaginary parts of the eigenvalues coalesce at this point. The EPs have been observed in many photonic systems, such as optical microcavities [29,30], coupled optical waveguides [31–33], photonic crystal slabs [34–37], and unidirectionally coupled resonators [38,39]. Many novel properties are also found at or near the EPs, such as loss-induced suppression and revival of lasing [40–42], unidirectional transmission or reflection [43–48], topological chirality [49–51], and laser mode selectivity [52–54]. Recently, the photonic nanostructures, which sustain higher-order EPs, have been demonstrated to be achievable and can be used for ultrasensitive nanoparticle sensing [55–61]. However, these nanosystems, which cannot create single-handed superchiral near fields, are not suitable for chiral discrimination. It is therefore relevant to ask whether strong superchiral fields can be created and the ultrasensitive chiral detection can be realized with the help of EPs.

In this Letter, we experimentally demonstrate a new type of EP called the radiation vector EP. This type of EP is created by suitably tuning the coupling strength between two orthogonal polarization modes and their radiation

losses in the photonics crystal slab. The eigenstate of this vector EP possesses strong and homogeneous superchiral fields. Based on the temporal coupled-mode theory, we find that two orthogonal polarization modes are nearly coupled to the opposite output ports at the vector EP. In this case, the strong superchiral fields can be generated near the photonic crystal slab excited with two beams of lights coming from opposite directions. Thus, our study opens up a new way for ultrasensitive detecting of molecular chirality.

We consider a photonic crystal slab with a square array of cylindrical holes (periodicity a , diameter d , and thickness h) coated on a substrate, as shown in Fig. 1(a). The refractive indexes of the background, photonic crystal slab, and substrate are labeled by n_b , n_p , and n_s , respectively. At the Γ point of the Brillouin zone, the system processes C_{4v} symmetry, where both one- and two-dimensional irreducible representations exist. Based on the symmetry arguments, only doubly degenerate Bloch modes can couple with free space, which gives rise to radiation losses. We first consider the structure, which is symmetric with respect to the $z = 0$ plane ($n_b = n_s$). For such a structure, the Bloch modes can be classified into two types with symmetric (TE-like) and antisymmetric (TM-like) distributions of electric fields. By tuning the diameter of the cylindrical hole (d) and the thickness of the photonic crystal slab (h), a pair of doubly degenerated TM- and TE-like modes can be spectrally close to each other and far from other modes. In this case, the system can be effectively described by a 4×4 non-Hermitian Hamiltonian (at the Γ point in the Brillouin zone),

$$H_{\text{sym}} = \begin{bmatrix} \omega_{\text{TE}}^1 + i\gamma_{\text{TE}}^1 & 0 & 0 & 0 \\ 0 & \omega_{\text{TM}}^1 + i\gamma_{\text{TM}}^1 & 0 & 0 \\ 0 & 0 & \omega_{\text{TE}}^2 + i\gamma_{\text{TE}}^2 & 0 \\ 0 & 0 & 0 & \omega_{\text{TM}}^2 + i\gamma_{\text{TM}}^2 \end{bmatrix}, \quad (1)$$

with $\omega_{\text{TE(TM)}}^i$ and $\gamma_{\text{TE(TM)}}^i$ ($i = 1, 2$) being the resonant frequency and the decay rate of the degenerated TE-like (TM-like) modes. Moreover, these parameters satisfy the relationship of $\omega_{\text{TE(TM)}}^1 = \omega_{\text{TE(TM)}}^2$ and $\gamma_{\text{TE(TM)}}^1 = \gamma_{\text{TE(TM)}}^2$.

By breaking the up-down symmetry ($n_b \neq n_s$), the orthogonal TE- and TM-like modes can couple with each other. In this case, the effective Hamiltonian of the system can be written as

$$H_{\text{asym}} = \begin{bmatrix} \omega_{\text{TE}}^1 + i\gamma_{\text{TE}}^1 & \kappa & 0 & 0 \\ \kappa^* & \omega_{\text{TM}}^1 + i\gamma_{\text{TM}}^1 & 0 & 0 \\ 0 & 0 & \omega_{\text{TE}}^2 + i\gamma_{\text{TE}}^2 & \kappa \\ 0 & 0 & \kappa^* & \omega_{\text{TM}}^2 + i\gamma_{\text{TM}}^2 \end{bmatrix}, \quad (2)$$

where κ quantifies the coupling strength, which can be tuned by changing the background refractive index n_b to control the breaking degree of the up-down symmetry. In this case, the interaction Hamiltonian $[0, \kappa; \kappa^*, 0]$ is a Hermitian operator because the interaction between the

TE- and TM-like modes is caused mainly by the evanescent field instead of far-field coupling via the radiation continuum. By tuning the coupling strength between the orthogonal polarization modes and their radiation losses (through changing the geometric parameters of the system),

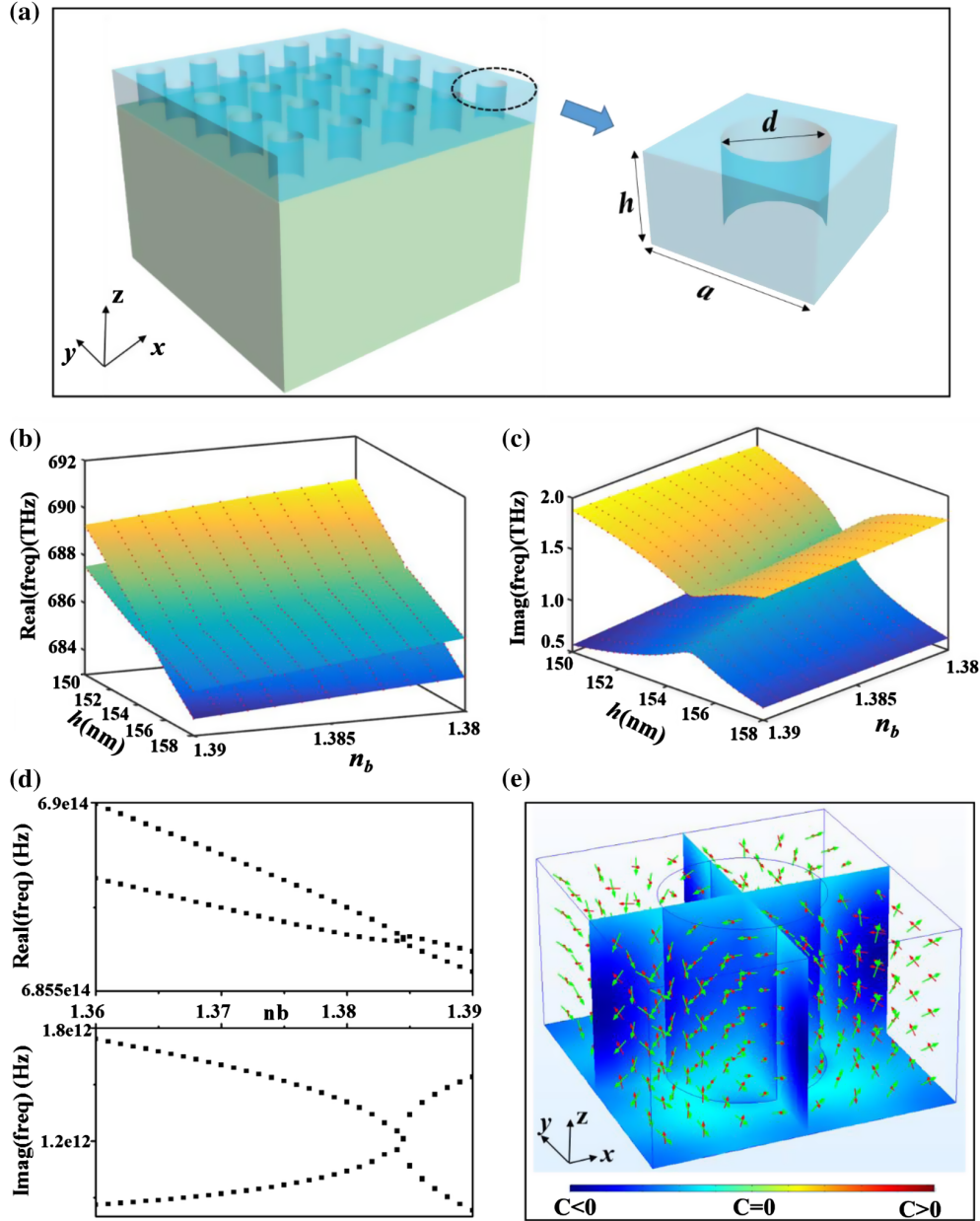


FIG. 1. (a) Diagram of the asymmetric photonic crystal slab. The (b) real and (c) imaginary parts of the eigenvalues for the system in the two parameters space, where the background refractive index and the thickness of the photonic crystal slab are swept. Other parameters are chosen as $a = 259$ nm, $d = 136$ nm, $n_p = 2.02$, and $n_s = 1.47$, respectively. (d) The real and imaginary parts of eigenvalues for the system as a function of the refractive index of the background medium when the thickness of the photonic crystal slab is fixed at $h = 154.2$ nm. (e) The optical chirality of the eigenmode at the vector EP. The red and green arrows correspond to the real and imaginary parts of the electric and magnetic fields.

the eigenvectors of H_{asym} can coalesce, giving rise to one pair of degenerated exceptional points. Such EPs are very different from that existing in the symmetric photonic crystal slab described in Ref. [34], where only TE-like modes are coupled. Here, our proposed EP is formed by two orthogonal polarization modes in the asymmetric photonic crystal slab, and it can be called the radiation vector EP.

Figures 1(b) and 1(c) show the real and imaginary parts of the band structure in the two-parameter space (each band

is doubly degenerated), where the refractive index of the background and thickness of the photonic crystal slab are swept. The remained parameters are chosen to be $a = 259$ nm, $d = 136$ nm, $n_p = n(\text{Si}_3\text{N}_4) = 2.02$, and $n_s = n(\text{Si}_2\text{O}_3) = 1.47$, respectively. The eigenvalues of the system are calculated by the eigenfrequency solver of COMSOL Multiphysics. It is clearly shown that both the real and imaginary parts of the eigenspectra possess the characteristics of a self-intersecting Riemann surface.

The EP marks the branch point where the Riemann surface splits. In Fig. 1(d), we further plot the real and imaginary parts of eigenvalues for the system as a function of the background refractive index when the thickness of the photonic crystal slab is fixed as $h = 154.2$ nm. It proves the existence of the EP when the background refractive index is set as $n_b = 1.3845$ (both the real and imaginary parts of eigenvalue being identical). Except for the square-root dispersion around the EP, the other important feature of the EP is that the corresponding eigenstates should also be coalesced. In Sec. I of the Supplemental Material [62], we present the numerical results of eigenfield distribution with different background mediums. We found that the eigenfield distribution for the two hybridized eigenstates becomes more and more similar to each other with the system approaching the exceptional point, which demonstrates the coalesce of eigenvectors.

This vector EP possesses a potential application for the realization of strong and single-handed superchiral fields. Other previous work [20] have proved that the excitation of TE (or electric) and TM (or magnetic) modes with $\pi/2$ phase shift is necessary to achieve the spatially homogeneous superchiral fields (locally displaying greater optical chirality than CPLs). In this consideration, our proposed vector EP may become a suitable candidate for this purpose. This is because the eigenmode of our designed vector EP [$\psi(\text{EP})$] ($\psi = [E_x, E_y, E_z, H_x, H_y, H_z]$) can be expressed as $\psi(\text{EP}) = \psi(\text{TE}) - i\psi(\text{TM})$. Taking the x -polarized case, for example, close to the central plane, the $\psi(\text{TE})$ and $\psi(\text{TM})$ take the forms of $\psi(\text{TE}) = [E_x^{(\text{TE})}, 0, 0, 0, 0, H_z^{(\text{TE})}]$ and $\psi(\text{TM}) = [0, 0, E_z^{(\text{TM})}, H_x^{(\text{TM})}, 0, 0]$, respectively. Thus, at the EP, the modal electric fields possess a large component parallel to the magnetic fields. The blue and green arrows in Fig. 1(e) show the real part of electric fields and the imaginary part of magnetic fields in a unit cell of the photonic crystal slab for the EP. At each location, the electric field has a large component parallel to the magnetic field. Such a phenomenon is absent if the mode is purely TE or TM polarized. From the definition $C = -\epsilon_0\omega\text{Im}(E^*B)/2$, these parallel and 90° out-of-phase electric and magnetic fields lead to a uniform and single-handed optical chirality field. Consequently, net superchiral fields may be produced by effectively exciting the photonic crystal slab at the vector EP. In this case, our designed vector EP can be used for ultrasensitive chiral detection.

To verify our theoretical design of the vector EP, we fabricate a Si_3N_4 photonic crystal slab on top of the silica substrate using electron beam lithography (see Sec. II in the Supplemental Material for details [62]). Scanning electron microscope images (both side and top views) of the sample are shown in Fig. 2(a). The sample is about $50 \times 50 \mu\text{m}^2$ and the period of the square lattice is $a = 259$ nm. The thickness and diameter of the cylindrical holes are $h = 154$ and $d = 136$ nm, respectively. These parameters are nearly

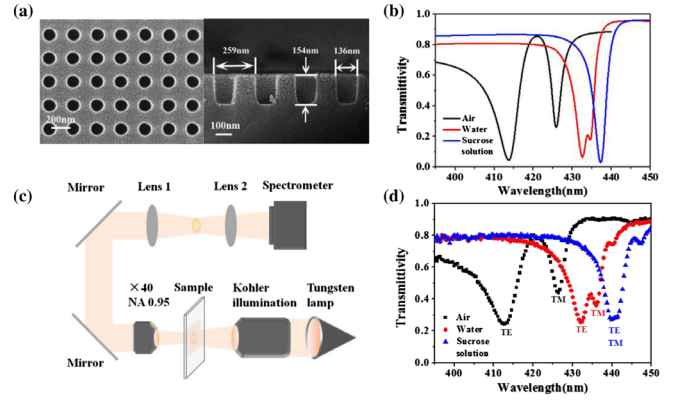


FIG. 2. (a) Side and top views of the scanning electron microscope images for the fabricated sample. The geometric parameters of the fabricated samples are, $a = 259$, $d = 136$, and $h = 154$ nm, respectively. (b),(d) The calculated and measured transmission spectra of the structure possessing the vector EP. The black, red, and blue lines and dots correspond to the conditions with the structure immersing into air, water, and sucrose solution, respectively. (c) Experimental setups for the measurement of transmission spectra.

identical with the structure, sustaining the vector EP discussed above. The only difference is that the absorption loss of the Si_3N_4 photonic crystal slab should be considered in the real experiments, where the refractive index of Si_3N_4 is chosen as $n(\text{Si}_3\text{N}_4) = 2.02 + i0.003$. It is worthy to note that the vector EP still exists even if the photonic crystal slab possesses small intrinsic losses [see Figs. S2(a) and S2(b) in the Supplemental Material [62]]. Based on the eigenspectra calculation, we find that two modes can merge into one at the vector EP by increasing the background refractive index [shown in Fig. S2 [62] and Fig. 1(d)]. This special property can be illustrated through the calculated and measured transmission spectra.

We first calculated the transmission spectra of the above structure, where the photonic crystal slab is immersed into various background media (air, water, and sucrose solution). As shown in Fig. 2(b), the black line marks the transmission spectrum with the background medium being air. Two separated valleys correspond to the excitation of TE- and TM-like modes. Because of the intrinsic loss of the Si_3N_4 photonic crystal slab, the transmittivities at these two valleys are not equal to zero. The red and blue lines correspond to cases where the background media are water and sucrose solutions, respectively. We found that the two separated valleys get much closer when the system is immersed into water ($n_b = 1.33$). Finally, a single valley of the transmission spectrum appears when the refractive index of the background medium reaches $n_b = 1.385$. In this case, the vector EP is proved to be achieved.

To experimentally demonstrate the realization of the vector EP, the transmission spectra within different background media are measured by using the homemade experimental setup [63], as shown in Fig. 2(c). Details

of measurement system are provided in Sec. II in the Supplemental Material [62]. The measured transmission spectra are plotted in Fig. 2(d). We find that the two separated modes can coalesce into one when the concentration of sucrose solution reaches 75% ($n_b = 1.385$). The measured results with different concentration of sucrose solution are plotted in Fig. S3 [62]. This phenomenon possesses a good agreement with numerical results. The extra little dip (near 448 nm in 75% sucrose solution), which should not exist ideally, may result from the defect mode caused by fabrication errors or nonvertical illumination of the system. The lower Q factor (larger width of the transmission spectra) compared with the theoretical prediction may result from the finite size effect of samples (about $50 \times 50 \mu\text{m}^2$) and scattering losses caused by fabrication imperfections and disorders [64].

Although the eigenstate of our designed vector EP possesses single-handed optical chirality [shown in Fig. 1(e)], it is not a simple task to effectively excite it. This is because the asymmetric structures always support different near-field distributions and electromagnetic responses when they are excited from different directions [65]. In this case, how to excite the asymmetric photonic crystal slab to create the single-handed superchiral field at the vector EP is unclear.

In order to explore the excitation property of TE- and TM-like modes, we develop the temporal coupled-mode theory for the system with two resonance modes and a pair of radiation channels (up- and downward ports). The analytical model is given in Sec. S4 of the Supplemental Material [62]. By using the proposed temporal coupled-mode theory, the modal excitation with different incident wavelengths and directions can be clearly analyzed. Here, the used parameters are identical with the structure [used in Fig. 1(e)] possessing the vector EP. As shown in Fig. 3(a), we plot the variation of absolute values for the normalized excitation strength of TE-like (blue dot) and TM-like (red dot) modes as functions of the wavelength for the incident

plane wave propagating along the $+z$ direction (incident from the substrate). It is clearly shown that the TM-like mode is mainly excited at the vector EP and the excitation strength for the TE-like mode is minimum in this case. In contrast, when the incident light is coming from the $-z$ axis (incident from the background), the TE-like mode can be significantly excited and the TM-like mode is nearly not raised, as shown in Fig. 3(b). Consequently, it is clearly shown that the TM-like (TE-like) mode is significantly coupled to the upward (downward) port at the vector EP. In this case, the homogeneous superchiral fields cannot be created near the photonic crystal slab excited by a single beam of the plane wave coming from either the up- or downward port. Hence, a new excited method should be proposed to generate the single-handed superchiral field at the vector EP.

Based on the modal-coupling property at the vector EP, we design a feasible scheme to generate the single-handed superchiral field at the vector EP by using two beams of CPLs to excite the system from opposite directions, as shown in Fig. 4(a). Figure 4(b) shows the averaged enhancement of C/C_0 in the cylindrical hole of the photonic crystal slab with different thicknesses. C_0 is the averaged optical chirality of the CPL. We find that the maximal enhancement of optical chirality appears in the system sustaining the vector EP (blue line, $h = 154.2$ nm). In this case, the corresponding distribution of the enhancement factor for the optical chirality near the structure is plotted in Fig. 4(c). It is clearly shown that the single-handed superchiral field, which is consistent with the eigenstate at the vector EP [shown in Fig. 1(e)], is created. When the thickness of the photonic crystal slab deviated from that of the structure possessing the vector EPs, the enhancement factor of C/C_0 is decreased, as shown in Fig. 4(b) (black, red, green, and pink lines). From the above results, we find that our designed photonic crystal slab sustaining the vector EP can generate the maximal near-field optical chirality under two beams of excitation

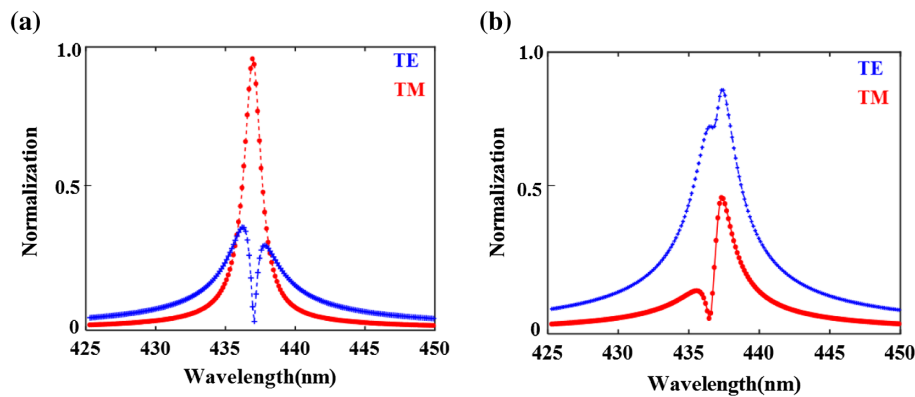


FIG. 3. The variation of absolute values for the normalized excitation strength of TE-like (blue dot) and TM-like (red dot) modes as functions of the wavelength for the incident light propagating along the $+z$ (a) and (b) $-z$ directions. The structural parameters are chosen as $a = 259$ nm, $d = 136$ nm, $n_p = 2.02$, $n_s = 1.47$, $n_b = 1.385$, and $h = 154.2$ nm, where the vector EP exists in the system.

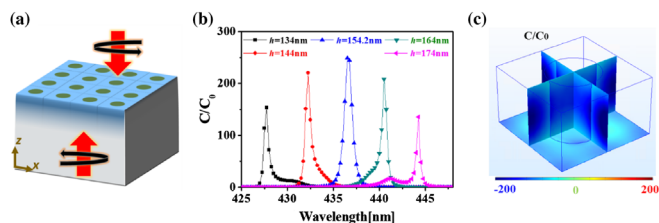


FIG. 4. (a) The scheme to generate the superchiral field at the vector EP by using two beams of CPL exciting the system from opposite directions. (b) The left chart shows the averaged enhancement of C/C_0 in the cylindrical hole of the photonic crystal slab with different thickness. The blue line corresponds to the structure sustaining EP with $h = 154.2$ nm. The black, red, green, and pink lines correspond to cases deviating from the vector EP. (c) Near-field distribution of optical chirality near the photonic crystal slab at the vector EP under two beams of excitation from opposite directions.

from opposite directions. Additionally, it is also important to note that the generated superchiral fields are also related to the initial relative phase of the two incident lights coming from opposite channels. This is because the relative phase between excited TE- and TM-like modes can also significantly influence the chirality of near fields. Only $\pi/2$ phase shift between TE- and TM-like modes can induce spatially homogeneous superchiral fields (see the Supplemental Material for details [62]). With the utilization of such strong and single-handed superchiral fields, our designed photonic crystal slab can be used to perform surface-enhanced fluorescence CD and Raman optical activity of chiral molecules, which are proportional to the optical chirality at the molecular positions.

In conclusion, we propose theoretically and demonstrate experimentally a new type of EP, which is called a radiation vector EP, to realize the strong superchiral fields for chiral molecular detection. By breaking the up-down symmetry, the TE- and TM-like modes can couple with each other and coalesce as the vector EP. With the help of temporal coupled-mode theory, we propose a scheme to generate a single-handed superchiral field near the photonic crystal slab at the vector EP, where two beams of light are used to excite the system from opposite directions. By using generated strong and homogenous superchiral fields, our designed photonic crystal slab could be an ideal platform to perform surface-enhanced fluorescence CD and Raman optical activity of chiral molecules. Moreover, by using the concept proposed in our Letter and the higher-order EP, we could design nanodevices with much higher sensitivity of chiral detection based on their resonance shifts. Some candidate systems include nanostructures with high-quality factors, such as the photonic crystal cavities, microspheres, or microdisks. Our findings may provide a guideline for the design of novel chiral nanosensors for applications in the fields of biomedicine and pharmaceuticals.

This work was supported by the National Natural Science Foundation of China (Grant No. 91850205) and the National Key R & D Program of China under Grant No. 2017YFA0303800.

*These authors contributed equally to this work.

†To whom all correspondence should be addressed.

zhangxd@bit.edu.cn

- [1] N. Berova, P.L. Polavarapu, K. Nakanishi, and W. Woody, *Comprehensive Chiroptical Spectroscopy* (Wiley, New York, 2012).
- [2] K. W. Busch and M. A. Busch, *Chiral Analysis* (Elsevier, Amsterdam, 2006).
- [3] H. J. Rhee, Y.-G. June, J.-S. Lee, K.-K. Lee, J.-H. Ha, Z. H. Kim, S.-J. Jeon, and M. Cho, *Nature (London)* **458**, 310 (2009).
- [4] D. Patterson, M. Schnell, and J. M. Doyle, *Nature (London)* **497**, 475 (2013).
- [5] D. Sofikitis, L. Bougas, G. E. Katsoprinakis, A. K. Spiliotis, B. Loppinet, and T. P. Rakitxis, *Nature (London)* **514**, 76 (2014).
- [6] G. D. Fasman, *Circular Dichroism and the Conformational Analysis of Biomolecules* (Plenum, New York, 1996).
- [7] G. H. Wagniere, *On Chirality and the Universal Asymmetry: Reflections on Image and Mirror Image* (VHCA with Wiley-VCH, Zurich, 2007).
- [8] B. M. Maoz, Y. Chaikin, A. B. Tesler, O. B. Elli, Z. Fan, A. O. Govorov, and G. Markovich, *Nano Lett.* **13**, 1203 (2013).
- [9] W. Ma, H. Kuang, L. Xu, L. Ding, C. Xu, L. Wang, and N. A. Kotov, *Nat. Commun.* **4**, 2689 (2013).
- [10] Y. Zhao, A. N. Askarpour, L. Sun, J. Shi, X. Li, and A. Alu, *Nat. Commun.* **8**, 14180 (2017).
- [11] E. Mohammadi, K. L. Tsakmakidis, A. N. Askarpour, P. Dehkoda, A. Tavakoli, and H. Altug, *ACS Photonics* **5**, 2669 (2018).
- [12] Y. Tang and A. E. Cohen, *Phys. Rev. Lett.* **104**, 163901 (2010).
- [13] Y. Tang and A. E. Cohen, *Science* **332**, 333 (2011).
- [14] C. He, G. Yang, Y. Kuai, S. Shan, L. Yang, J. Hu, D. Zhang, Q. Zhang, and G. Zou, *Nat. Commun.* **10**, 2093 (2019).
- [15] E. Hendry, T. Carpy, J. Johnston, M. Popland, R. V. Mikhaylovskiy, A. J. Laphorn, S. M. Kelly, L. D. Barron, N. Gadegaard, and M. Kadodwala, *Nat. Nanotechnol.* **5**, 783 (2010).
- [16] M. Schäferling, D. Dregely, M. Hentschel, and H. Giessen, *Phys. Rev. X* **2**, 031010 (2012).
- [17] M. Schäferling, X. Yin, and H. Giessen, *Opt. Express* **20**, 26326 (2012).
- [18] T. J. Davis and E. Hendry, *Phys. Rev. B* **87**, 085405 (2013).
- [19] A. Vazquez-Guardado and D. Chanda, *Phys. Rev. Lett.* **120**, 137601 (2018).
- [20] A. Garcia-Etxarri and J. A. Dionne, *Phys. Rev. B* **87**, 235409 (2013).
- [21] R. Y. Wang *et al.*, *J. Phys. Chem. C* **118**, 9690 (2014).
- [22] R. Tullius, A. S. Karimullah, M. Rodier, B. Fitzpatrick, N. Gadegaard, L. D. Barron, V. M. Rotello, G. Cooke,

- A. Laphorn, and M. Kadodwala, *J. Am. Chem. Soc.* **137**, 8380 (2015).
- [23] F. Graf, J. Feis, X. Garcia-Santiago, M. Wegener, C. Rockstuhl, and I. Fernandez-Corbaton, *ACS Photonics* **6**, 482 (2019).
- [24] T. Wu, J. Ren, R. Wang, and X. Zhang, *J. Phys. Chem. C* **118**, 20529 (2014).
- [25] W. Zhang, T. Wu, R. Wang, and X. Zhang, *J. Phys. Chem. C* **121**, 666 (2017).
- [26] C. M. Bender and S. Böttcher, *Phys. Rev. Lett.* **80**, 5243 (1998).
- [27] N. Moiseyev, *Non-Hermitian Quantum Mechanics* (Cambridge Univ. Press, Cambridge, England, 2011).
- [28] M. A. Miri and A. Alù, *Science* **363**, eaar7709 (2019).
- [29] H. Cao and J. Wiersig, *Rev. Mod. Phys.* **87**, 61 (2015).
- [30] B. Peng, Ş. K. Özdemir, F. Lei, F. Monifi, M. Gianfreda, G. L. Long, S. Fan, F. Nori, C. M. Bender, and L. Yang, *Nat. Phys.* **10**, 394 (2014).
- [31] S. Klaiman, U. Günther, and N. Moiseyev, *Phys. Rev. Lett.* **101**, 080402 (2008).
- [32] C. E. Ruter, K. G. Makris, R. El-Ganainy, D. N. Christodoulides, M. Segev, and D. Kip, *Nat. Phys.* **6**, 192 (2010).
- [33] C. Hahn, Y. Choi, J. W. Yoon, S. H. Song, C. H. Oh, and P. Berini, *Nat. Commun.* **7**, 12201 (2016).
- [34] B. Zhen, C. W. Hsu, Y. Igarashi, L. Lu, I. Kaminer, A. Pick, S.-L. Chua, J. D. Joannopoulos, and M. Soljačić, *Nature (London)* **525**, 354 (2015).
- [35] Z. Lin, A. Pick, M. Loncar, and A. W. Rodriguez, *Phys. Rev. Lett.* **117**, 107402 (2016).
- [36] K.-H. Kim, M.-S. Hwang, H.-R. Kim, J.-H. Choi, Y.-S. No, and H.-G. Park, *Nat. Commun.* **7**, 13893 (2016).
- [37] H. Zhou, C. Peng, Y. Yoon, C. W. Hsu, K. A. Nelson, L. Fu, J. D. Joannopoulos, M. Soljačić, and B. Zhen, *Science* **359**, 1009 (2018).
- [38] L. Chang, X. Jiang, S. Hua, C. Yang, J. Wen, L. Jiang, G. Li, G. Wang, and M. Xiao, *Nat. Photonics* **8**, 524 (2014).
- [39] N. Caselli *et al.*, *Nat. Commun.* **9**, 396 (2018).
- [40] Z. J. Wong, Y.-L. Xu, J. Kim, K. O'Brien, Y. Wang, L. Feng, and X. Zhang, *Nat. Photonics* **10**, 796 (2016).
- [41] B. Peng, Ş. K. Özdemir, S. Rotter, H. Yilmaz, M. Liertzer, F. Monifi, C. M. Bender, F. Nori, and L. Yang, *Science* **346**, 328 (2014).
- [42] M. Liertzer, L. Ge, A. Cerjan, A. D. Stone, H. E. Tureci, and S. Rotter, *Phys. Rev. Lett.* **108**, 173901 (2012).
- [43] K. G. Makris, R. El-Ganainy, D. N. Christodoulides, and Z. H. Musslimani, *Phys. Rev. Lett.* **100**, 103904 (2008).
- [44] A. Guo, G. J. Salamo, D. Duchesne, R. Morandotti, M. Volatier-Ravat, V. Aimez, G. A. Siviloglou, and D. N. Christodoulides, *Phys. Rev. Lett.* **103**, 093902 (2009).
- [45] Y. D. Chong, L. Ge, and A. D. Stone, *Phys. Rev. Lett.* **106**, 093902 (2011).
- [46] Z. Lin, H. Ramezani, T. Eichelkraut, T. Kottos, H. Cao, and D. N. Christodoulides, *Phys. Rev. Lett.* **106**, 213901 (2011).
- [47] A. Regensburger, C. Bersch, M.-A. Miri, G. Onishchukov, D. N. Christodoulides, and U. Peschel, *Nature (London)* **488**, 167 (2012).
- [48] J. W. Yoon *et al.*, *Nature (London)* **562**, 86 (2018).
- [49] J. Doppler, A. A. Mailybaev, J. Böhm, U. Kuhl, A. Girschik, F. Libisch, T. J. Milburn, P. Rabl, N. Moiseyev, and S. Rotter, *Nature (London)* **537**, 76 (2016).
- [50] H. Xu, D. Mason, L. Jiang, and J. G. E. Harris, *Nature (London)* **537**, 80 (2016).
- [51] C. Dembowski, H. D. Graf, H. L. Harney, A. Heine, W. D. Heiss, H. Rehfeld, and A. Richter, *Phys. Rev. Lett.* **86**, 787 (2001).
- [52] H. Hodaei, M.-A. Miri, M. Heinrich, D. N. Christodoulides, and M. Khajavikhan, *Science* **346**, 975 (2014).
- [53] L. Feng, Z. J. Wong, R.-M. Ma, Y. Wang, and X. Zhang, *Science* **346**, 972 (2014).
- [54] E. Lafalce, Q. Zeng, C. H. Lin, M. J. Smith, S. T. Malak, J. Jung, Y. J. Yoon, Z. Lin, V. V. Tsukruk, and Z. V. Vardeny, *Nat. Commun.* **10**, 561 (2019).
- [55] J. Wiersig, *Phys. Rev. Lett.* **112**, 203901 (2014).
- [56] G. Q. Zhang, Y. P. Wang, and J. Q. You, *Phys. Rev. A* **99**, 052341 (2019).
- [57] Z.-P. Liu, J. Zhang, Ş. K. Özdemir, B. Peng, H. Jing, X.-Y. Lü, C.-W. Li, L. Yang, F. Nori, and Y.-x. Liu, *Phys. Rev. Lett.* **117**, 110802 (2016).
- [58] W. Chen, S. K. Özdemir, G. Zhao, J. Wiersig, and L. Yang, *Nature (London)* **548**, 192 (2017).
- [59] H. Hodaei *et al.*, *Nature (London)* **548**, 187 (2017).
- [60] H. K. Lau and A. A. Clerk, *Nat. Commun.* **9**, 4320 (2018).
- [61] S. Wang, B. Hou, W. Lu, Y. Chen, Z. Q. Zhang, and C. T. Chan, *Nat. Commun.* **10**, 832 (2019).
- [62] See Supplemental Material at <http://link.aps.org/supplemental/10.1103/PhysRevLett.124.083901> for the numerical results of the eigenfield distribution with different background media, the details of the sample fabrication and transmission spectrum measurement, the influence of intrinsic losses of Si₃N₄ on the vector EP, the measured transmission spectra with different concentration of sucrose solution, the details of the temporal coupled-mode theory and the influence of the initial relative phase of the incident light coming from two channels on the excitation of the vector EP.
- [63] J. C. Jin, X. Yin, L. Ni, M. Soljačić, B. Zhen, and C. Peng, *Nature (London)* **574**, 501 (2019).
- [64] D. L. Sounas and A. Alù, *Phys. Rev. Lett.* **118**, 154302 (2017).
- [65] Y. Zhang, A. Chen, W. Liu, C. W. Hsu, B. Wang, F. Guan, X. Liu, L. Shi, L. Lu, and J. Zi, *Phys. Rev. Lett.* **120**, 186103 (2018).